

## BULK AMORPHOUS MAGNETIC MATERIALS

N. Lupu, H. Chiriac

National Institute of R&D for Technical Physics, 47 Mangeron Blvd., 6600 Iasi, Romania

The relationship between microstructure and magnetic properties of melt-spun ribbons with thicknesses up to 150  $\mu\text{m}$  and cast rods having up to 3 mm in diameter prepared by mould casting and suction casting, with nominal compositions  $\text{Fe}_{56}\text{Co}_7\text{Ni}_7\text{Zr}_6\text{M}_{1.5}\text{Nb}_{2.5}\text{B}_{20}$  ( $\text{M} = \text{Zr}$ ,  $\text{Ti}$ ,  $\text{Ta}$  or  $\text{Mo}$ ) and  $\text{Nd}_{90-x}\text{Fe}_x\text{Si}_{10-y}\text{Al}_y$  ( $x = 35 - 50$ ;  $y = 0 - 10$ ) was investigated. Saturation magnetizations up to 1.1 T, coercive fields of about 5 A/m, magnetic permeability of 25000-30000 in the as-cast state were measured for Fe-based amorphous alloys. The large values of the intrinsic coercive field over 300 kA/m at room temperature and over 600 kA/m at 200 K, measured in a maximum field of 1 T for Nd-Fe-based "X-ray amorphous" alloys, and the strong dependence of the coercive field on temperature and cooling rate are ascribed to the development in the amorphous matrix of a metastable or non-equilibrium magnetic phase consisting in very small clusters whose sizes are below 5-10 nm. The magnetic properties of Nd-Fe-based bulk amorphous alloys are very sensitive to the Nd:Fe ratio, the addition element, the method of preparation, the thickness of the samples and the type of thermal or thermomagnetic treatment.

(Received February 5, 2002; accepted May 15, 2002)

*Keywords:* Bulk amorphous alloys, Soft magnetic alloys, Coercive field-thickness dependence, High-coercivity materials

### 1. Introduction

The interest in glass-forming alloys, which vitrify at relatively low cooling rates ( $10^0 - 10^2$  K/sec) from the molten state compared with conventional rapidly quenched metallic glasses, has grown in the last years. Owing to their resistance to crystallization, these easy glass-forming alloys can be cast in bulk shapes with dimensions of millimeters. The development of these new amorphous alloys may contribute widely to the understanding of the physical processes that take place in the supercooled liquid region and to the amorphization process itself due to the high thermal stability of the supercooled liquid region, making also possible the design of new applications based on their ability to be prepared in three-dimensional shapes.

The history of bulk metallic glasses is dating back in time [1]. Despite of that, no ferromagnetic bulk metallic glasses were successfully synthesized before 1995. Inoue and co-workers from Tohoku University, Sendai, Japan announced in 1995 the preparation of the first bulk amorphous alloys with soft magnetic properties at room temperature in Fe-(Al,Ga)-(P,C,B,Si) multicomponent system [2,3] and one year later the first bulk amorphous hard magnetic alloys synthesized in (Nd,Pr)-Fe-Al system [4,5]. These alloys are very attractive for the subsequent development of the basic science and engineering applications, but so far as we know the mechanisms governing their magnetic behavior are not well known and understood.

This paper is restricted to the magnetic properties of two families of bulk amorphous alloys that we consider representative for this field: soft magnetic (Fe,Co,Ni)-Zr-B based alloys and room temperature high-coercivity Nd-Fe-(Al,Si) alloys. Emphasis is placed on the interplay between the atomic structure and the magnetic properties. The influence of the composition, preparation technique (cooling rate), annealing and the on-set of crystallization on magnetic properties of Fe-based and Nd-Fe-based bulk amorphous alloys is investigated. Brief remarks conclude the paper. Finally, some potential applications are suggested.

## 2. Experimental

Master alloys of 5-10 g each were prepared by arc melting pure elements (99.99 %) in an argon atmosphere. Ribbons with thicknesses between 20 and 200  $\mu\text{m}$  and widths of 2-5 mm were obtained by maintaining constant the crucible orifice size and the ejection pressure and changing the wheel velocity between 30 and 2.5 m/sec.  $\text{Fe}_{56}\text{Co}_7\text{Ni}_7\text{Zr}_6\text{M}_{1.5}\text{Nb}_{2.5}\text{B}_{20}$  ( $\text{M} = \text{Zr}, \text{Ti}, \text{Ta}, \text{Mo}$ ) amorphous cast rods with diameters between 0.5 and 3 mm,  $\text{Nd}_{90-x}\text{Fe}_x\text{Al}_{10}$  ( $x = 20 - 50$ ) amorphous cast rods with diameters of 1 and 1.5 mm and  $\text{Fe}_{56}\text{Co}_7\text{Ni}_7\text{Zr}_{7.5}\text{Nb}_{2.5}\text{B}_{20}$  amorphous cast rings with  $D_{\text{int}} = 6$  mm,  $D_{\text{ext}} = 10$  mm and  $t = 1$  mm were prepared by Cu mould casting method. The method consists in applying an overpressure at the upper part of the molten alloy and forcing the melt to “flow” in a water-cooled Cu mould having different cavities within. Amorphous cylinders with diameters between 0.6 and 3 mm from  $\text{Nd}_{90-x}\text{Fe}_x\text{Al}_{10-y}\text{Si}_y$  alloys ( $x = 20 - 50$ ;  $y = 0 - 10$ ) were produced by suction casting method. The master alloy is arc melted in a water-cooled Cu crucible and sucked up thereafter in a cooled Cu mould having inside different shaped cavities.

Qualitative information about the structure of Fe-based and Nd-Fe based ribbons and cast samples were obtained by X-ray diffraction (XRD) using Cu-K $\alpha$  and Mo-K $\alpha$  radiations. The structure was checked on both sides as well as on powders obtained by milling the ribbons, while XRD investigations on cast samples (rods or rings) were performed using powders obtained after crushing the rod into small pieces and then milling. Neutron diffraction measurements have been made on amorphous  $\text{Nd}_{90-x}\text{Fe}_x\text{Al}_{10}$  ( $x = 20 - 60$ ) at 12 temperatures between 15 and 773 K. Total structure factors,  $S(Q)$  have been measured for melt-spun ribbons with thicknesses between 20 and 120  $\mu\text{m}$  and cast rods with diameters no larger than 2 mm by powder diffraction using the SLAD diffractometer at the Studsvik Neutron Research Laboratory. The data have been modeled using the reverse Monte Carlo (RMC) method [6] under the assumption that the atomic structure is completely disordered. In the reverse Monte Carlo simulations reported here, systems containing 2000 – 2500 particles were used. The input experimental data was  $S(Q)$ . The experimental number density,  $\rho$ , was 0.055  $\text{\AA}^{-3}$ . Closest-approach distances were determined on the basis of the corresponding experimental data. All calculations were started from hard sphere random configurations. For reaching equilibrium (the closest fit to the experiment), 6.5-8.5  $\times 10^6$  accepted moves had to be completed.

Data about glass transition temperature ( $T_g$ ), crystallization and melting temperature, thermal stability of the supercooled liquid region and the evolution of the crystallization process with the composition and samples thickness were acquired from calorimetric measurements (DSC) performed at a heating rate of 20 K/sec. The difference between Fe-based and Nd-Fe-based amorphous alloys consists in the position of the glass-transition temperature relative to the crystallization temperature: while for Fe-based,  $T_g$  is situated below  $T_x$ , like in most of the previous studied amorphous alloys, for Nd-Fe-based  $T_g$  can not be evidenced on DSC curves, because it is located between  $T_x$  and  $T_m$  and the large glass-forming ability is given by the reduced crystallization temperature ( $T_x/T_m$ ). DC-magnetic measurements above room temperature but not exceeding 1100 K, at applied magnetic fields limited to 1260 kA/m, were carried out using a homemade vibrating sample magnetometer (VSM). The variation of the magnetization and coercive field below room temperature (5 – 300 K) was studied in fields up to 800 kA/m using a superconducting quantum interference device (SQUID) magnetometer and for maximum applied fields of 7.2 MA/m using an Oxford MagLab VSM. The magnetic field was applied in the axial direction of the samples. Each sample was thermally demagnetized prior to recording the magnetic measurements. The magnetic permeability ( $\mu_e$ ) and the electrical resistivity ( $\rho_{\text{RT}}$ ) of the Fe-based amorphous alloys were determined by using an AC fluxmetric method in a maximum applied field of 1000 A/m, while the saturation magnetostriction constant ( $\lambda_s$ ) was measured by the small angle magnetisation rotation (SAMR) method.

## 3. Results and discussions

### 3.1 Soft magnetic bulk amorphous alloys

DSC curves exhibit one endothermic peak corresponding to the glass transition for  $\text{Fe}_{56}\text{Co}_7\text{Ni}_7\text{Zr}_6\text{Nb}_{2.5}\text{M}_{1.5}\text{B}_{20}$  amorphous alloys. The existence of one exothermic peak for the

amorphous alloys containing 1.5 at. % Zr, Ta or Mo and a shifted peak for  $\text{Fe}_{56}\text{Co}_7\text{Ni}_7\text{Zr}_6\text{Nb}_{2.5}\text{Ti}_{1.5}\text{B}_{20}$  amorphous alloy indicates one stage crystallization process for the former alloys and two-stage crystallization for the last one [7]. The substitution of 1.5 at. % Zr with Ti, Ta or Mo leads to the increase of the resistance of the supercooled liquid region against crystallization and consequently the maximum thickness for which the bulk samples are still amorphous increases about 2 times, from 1.6 mm for  $M = \text{Zr}$  to 3 mm for  $M = \text{Ti, Ta and Mo}$ . Although the replacement of Zr with Ti, Ta or Mo causes the decrease of the glass transition temperature,  $\Delta T_x$  increases with 10 degrees from 80 to 90 K [8].

Another evidence for the formation of the amorphous phase in  $(\text{Fe,Co,Ni})_{70}(\text{Zr,M,Nb})_{10}\text{B}_{20}$  alloys is given by X-ray diffraction patterns, which indicate just one broad maximum characteristic to the amorphous phase and no sharp lines corresponding to crystalline phases for thick ribbons 150  $\mu\text{m}$  in thickness, regardless of their composition. The fully amorphous structure was also found in  $\text{Fe}_{56}\text{Co}_7\text{Ni}_7\text{Zr}_{7.5}\text{Nb}_{2.5}\text{B}_{20}$  bars with diameters up to 1.6 mm and rings with  $t = 1$  mm as well as in bars having diameters up to 3 mm prepared from  $\text{Fe}_{56}\text{Co}_7\text{Ni}_7\text{Zr}_6\text{Nb}_{2.5}\text{M}_{1.5}\text{B}_{20}$  ( $M = \text{Ti, Ta, Mo}$ ) alloys.

The existence of a single amorphous phase and no crystalline traces in the  $\text{Fe}_{56}\text{Co}_7\text{Ni}_7\text{Zr}_6\text{M}_{1.5}\text{Nb}_{2.5}\text{B}_{20}$  bulk amorphous samples is evidenced also by thermomagnetic measurements [9]. The first decrease of the magnetization to zero with the temperature increase gives the value of the Curie temperature of the amorphous phase (about 554 K) and proves the amorphicity of the sample. The magnetization starts to increase by the on-set of crystallization (about 860 K), reaches a maximum and decreases again to zero when the fully crystalline sample becomes paramagnetic, indicating a value around 1100 K for the Curie temperature of the crystalline alloy. The magnetization increases when the sample suffers a phase transition from amorphous to crystalline.

The change of the composition of the  $\text{Fe}_{56}\text{Co}_7\text{Ni}_7\text{Zr}_{7.5}\text{Nb}_{2.5}\text{B}_{20}$  basic alloy causes not just the increase of the glass-forming ability shown previously, but also the modification of the soft magnetic properties as it can be seen in Table 1. While the saturation magnetization does not change significantly by introduction of Ti, Ta or Mo instead of Zr in the basic alloy, the magnetic permeability decreases from 21500 for the  $\text{Fe}_{56}\text{Co}_7\text{Ni}_7\text{Zr}_{7.5}\text{Nb}_{2.5}\text{B}_{20}$  amorphous ribbons having 35  $\mu\text{m}$  in thickness to 17000 for the  $\text{Fe}_{56}\text{Co}_7\text{Ni}_7\text{Zr}_6\text{Nb}_{2.5}\text{Mo}_{1.5}\text{B}_{20}$  amorphous ribbons with the same thickness. The Curie temperature increases and coercive field decreases by the substitution of Zr with Ti, Ta or Mo.

Table 1. Soft magnetic characteristics of the  $\text{Fe}_{56}\text{Co}_7\text{Ni}_7\text{Zr}_6\text{Nb}_{2.5}\text{M}_{1.5}\text{B}_{20}$  ( $M = \text{Zr, Ti, Ta, Mo}$ ) amorphous ribbons having 35  $\mu\text{m}$  in thickness.

	$\mu_0 M_s$ (T)	$H_c$ (A/m)	$\mu_e$ (500 Hz)	$T_c$ (K)
$M = \text{Zr}$	1.01	9.5	21,500	554
$M = \text{Ta}$	0.89	6.06	18,000	560
$M = \text{Ti}$	1.06	6.1	19,000	603
$M = \text{Mo}$	1.07	7.43	17,000	560

This behavior could also be explained on the basis of the increase of the thermal stability of the supercooled liquid region. The crystallization energy, determined by the area under the exothermic peak on DSC curves, is larger for amorphous alloys with Ti and Mo suggesting a higher degree of structural disorder and consequently the development of different magnetic structures more stable.

The large values of the magnetic permeability obtained for  $\text{Fe}_{56}\text{Co}_7\text{Ni}_7\text{Zr}_6\text{M}_{1.5}\text{Nb}_{2.5}\text{B}_{20}$  amorphous alloys are closely related to the high electrical resistivities ( $\rho_{\text{RT}}$ ) and to the relatively small saturation magnetostriction constant ( $\lambda_s$ ) measured in the as-cast state.  $\rho_{\text{RT}}$  increases from  $1.51 \cdot 10^{-8} \Omega \cdot \text{m}$  for  $M = \text{Zr}$  to  $2.08 \cdot 10^{-8} \Omega \cdot \text{m}$ ;  $1.87 \cdot 10^{-8} \Omega \cdot \text{m}$  and  $1.76 \cdot 10^{-8} \Omega \cdot \text{m}$  for  $M = \text{Ti, Ta and Mo}$ , respectively.  $\lambda_s$  ranges from  $7 \cdot 10^{-6}$  for  $\text{Fe}_{56}\text{Co}_7\text{Ni}_7\text{Zr}_{7.5}\text{Nb}_{2.5}\text{B}_{20}$  amorphous alloys to  $10 \cdot 10^{-6}$  for the amorphous alloys having Ti, Ta or Mo in composition. The small values of  $\lambda_s$  explain also the reduced values of the coercive field.

The improvement of the magnetic properties of  $\text{Fe}_{56}\text{Co}_7\text{Ni}_7\text{Zr}_6\text{M}_{1.5}\text{Nb}_{2.5}\text{B}_{20}$  amorphous alloys is obtained by choosing the suitable composition or by increasing the thickness of the samples, namely by attaining a high degree of structural relaxation in the as-cast state. Fig. 1 shows the behavior of the magnetic permeabilities at 500 Hz as a function of thickness for

$\text{Fe}_{56}\text{Co}_7\text{Ni}_7\text{Zr}_{7.5}\text{Nb}_{2.5}\text{B}_{20}$  melt-spun ribbons and cast rods. The increase of the amorphous ribbons thickness leads to the structural relaxation and consequently the permeability increases. The thicker amorphous ribbons the higher degree of structural relaxation and the better magnetic properties. The role of the eddy current in the amorphous ribbons with thicknesses up to  $150\ \mu\text{m}$  is very small and hence it could be neglected. The on-set of crystallization in ribbons with thicknesses larger than  $150\ \mu\text{m}$  results in the decrease of the magnetic permeability and in the displacement of the maximum of the permeability towards high-applied fields. The magnetic permeability of the  $\text{Fe}_{56}\text{Co}_7\text{Ni}_7\text{Zr}_{7.5}\text{Nb}_{2.5}\text{B}_{20}$  amorphous cast rods with diameters up to  $1.6\ \text{mm}$  is smaller than the values obtained for melt-spun amorphous ribbons. This behavior is related to the development of different magnetic domain structures in rods in comparison with ribbons due to the different cooling rates used in the preparation process and the difference between the amorphous samples dimensions. For  $\text{Fe}_{56}\text{Co}_7\text{Ni}_7\text{Zr}_{7.5}\text{Nb}_{2.5}\text{B}_{20}$  cast rod  $3\ \text{mm}$  in diameter, which is crystalline in the as-cast state, the magnetic permeability is very small. Thus, the good soft magnetic properties of  $\text{Fe}_{56}\text{Co}_7\text{Ni}_7\text{Zr}_6\text{M}_{1.5}\text{Nb}_{2.5}\text{B}_{20}$  bulk amorphous alloys are strongly related to the existence of the amorphous phase.

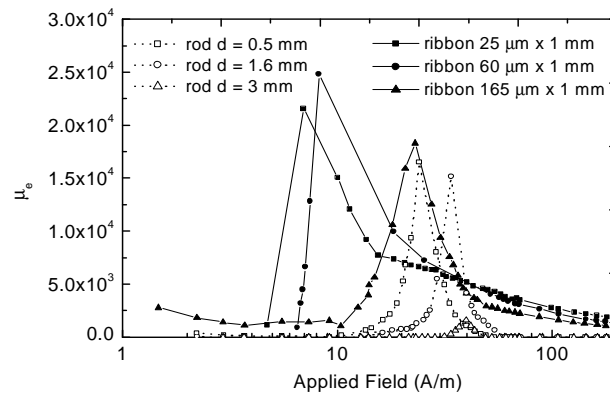


Fig. 1. Magnetic permeabilities (at 500 Hz) of  $\text{Fe}_{56}\text{Co}_7\text{Ni}_7\text{Zr}_{7.5}\text{Nb}_{2.5}\text{B}_{20}$  melt-spun ribbons and cast rods.

It is important to notice that at 10 kHz the magnetic permeability is the same for  $\text{Fe}_{56}\text{Co}_7\text{Ni}_7\text{Zr}_6\text{M}_{1.5}\text{Nb}_{2.5}\text{B}_{20}$  amorphous alloys in the shape of ribbons and bulk samples (rods or rings), while at 500 Hz they differ with about 35 %. This observation suggests bulk amorphous alloys as good for application at intermediary frequencies.

Structural relaxation of  $\text{Fe}_{56}\text{Co}_7\text{Ni}_7\text{Zr}_6\text{M}_{1.5}\text{Nb}_{2.5}\text{B}_{20}$  amorphous alloys can be also reached by annealing the amorphous samples at temperatures below glass transition temperature ( $T_g$ ). Treatments applied below  $753\ \text{K}$  (20 degrees below  $T_g$ ) leave the sample in the amorphous state and lead to the increase of the magnetic permeability while the magnetization remains almost the same as in the as-cast state. The subsequently increase of the annealing temperature results in the on-set of the nucleation leading to the decrease of the magnetic permeability and the increase of the magnetization. In the same time by increasing the annealing temperature the magnetization decreases but doesn't become zero, indicating a mixture of amorphous and crystalline phases. The coercive field exhibits initially a decrease with temperature and starts to increase when annealing temperature exceeds  $T_x$ , this increase being much pronounced for the basic alloy ( $M = \text{Zr}$ ). The precipitation of crystalline phases results in suddenly increase of the coercive field ( $H_c$ ).

Fig. 2 shows the modification of the shape of the hysteresis loops after thermal and thermomagnetic treatments for one thick amorphous ribbon ( $120\ \mu\text{m}$ ) prepared from the basic alloy  $\text{Fe}_{56}\text{Co}_7\text{Ni}_7\text{Zr}_{7.5}\text{Nb}_{2.5}\text{B}_{20}$ . The direction of the applied magnetic field is relative to the long axis of the ribbon.

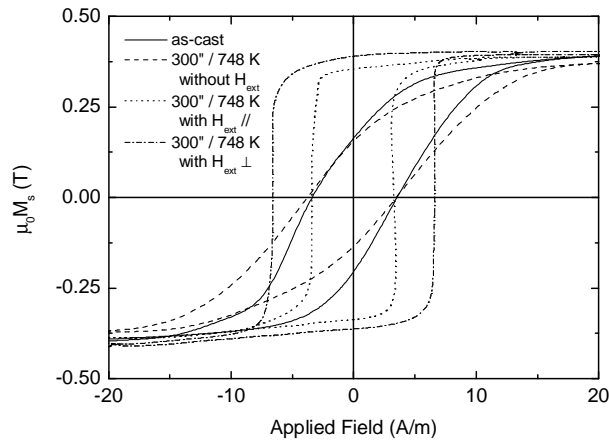


Fig. 2. The hysteresis loop shape dependence on the type of treatment for  $\text{Fe}_{56}\text{Co}_7\text{Ni}_7\text{Zr}_{7.5}\text{Nb}_{2.5}\text{B}_{20}$  amorphous alloys.

One observes that the rectangularity of the hysteresis loop as well as the saturation magnetization and coercive field are changing with the direction of the applied magnetic field. While the thermal treatment without magnetic field below  $T_g$  ( $= 773 \text{ K}$ ) leads to the slight increase of the coercive field and to the elongation of the hysteresis loop, the presence of an external magnetic field results in better magnetic properties, i.e. the better softness of the amorphous material. The best response is obtained when the applied field is parallel with the long axis of the ribbon because of the easy axis induced on the parallel direction with the applied field. When the external field is perpendicular to the ribbon long axis the induced anisotropy is smaller owing to the competition of the magnetoelastic anisotropy induced during the melt-spinning preparation process and oriented parallel with the long axis. Consequently, the coercive field increases. Further experimental work along this line is expected in the near future.

### 3.2 High-coercivity bulk amorphous alloys

The large glass-forming ability of  $\text{Nd}_{90-x}\text{Fe}_x(\text{Al},\text{Si})_{10}$  alloys is due to the high values of 0.8 to 0.92 of the reduced crystallization temperature ( $T_x/T_m$ , where  $T_x$  and  $T_m$  are crystallization and eutectic melting temperature, respectively). DSC curves indicate only one exothermic peak due to crystallization and neither endothermic reaction due to the glass transition nor the supercooled liquid region in the temperature range before crystallization [9]. The total replacement of Al with Si results in the decrease of the glass-forming ability and consequently the ability to fabricate bulk cast samples with fully amorphous structure is decreased. The increase of the Nd content (for 10 at. % Al), results in the enlargement of the glass-forming ability. The crystallization energy (the area under the exothermic peak) is higher for the melt-spun ribbons containing a higher amount of Fe in comparison with the rods due to the more disordered amorphous structure developed in the first ones. The crystallization energy doesn't change significantly as a function of the Fe content for  $\text{Nd}_{90-x}\text{Fe}_x\text{Al}_{10}$  thin ribbons 30  $\mu\text{m}$  thickness, whereas for cast rods it strongly decreases with the increase of the Fe content as a consequence of the decrease of the glass-forming ability. This behavior is explained by the insufficient cooling rates assured by the casting techniques for the alloys with larger contents of Fe and indicates a strong correlation between the composition, the cooling rate and the glass-forming ability for Nd-Fe-based ternary amorphous alloys.

In Fig. 3 are presented the neutron diffraction patterns taken at room temperature for  $\text{Nd}_{90-x}\text{Fe}_x\text{Al}_{10}$  ( $x = 35; 40; 50$ ) melt-spun ribbons with thicknesses of 25 and 120  $\mu\text{m}$ , respectively. Due to the decrease of the glass-forming ability, the  $\text{Nd}_{40}\text{Fe}_{50}\text{Al}_{10}$  ribbon 120  $\mu\text{m}$ , cannot be obtained fully amorphous.

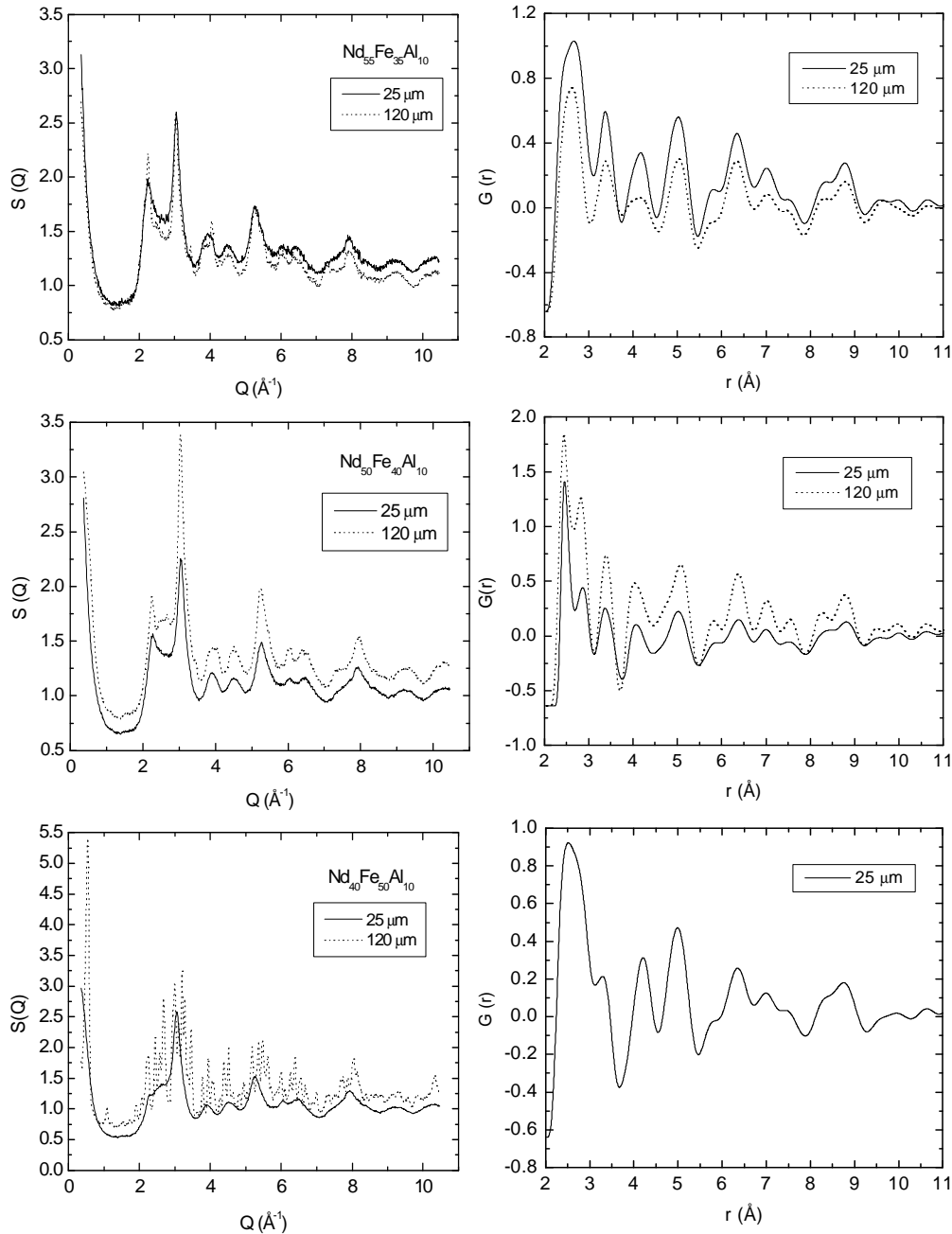


Fig. 3. Neutron diffraction pattern as a function of wavevector ,  $Q = 4\pi \sin \theta / \lambda$  , and reduced radial distribution function  $G(r) = 4\pi r^2 \rho(r)$  for  $\text{Nd}_{90-x}\text{Fe}_x\text{Al}_{10}$  melt-spun ribbons.

The split first peak and the pronounced structure at higher angles are features not present in the patterns for the other amorphous alloys with dense random packing disordered structures but they were observed in Nd-Fe binary amorphous alloys [10]. The split is more pronounced for the thicker ribbon than for the thin ones. We suppose this behavior being related to the more relaxed structure developed in thick ribbons. The reduced radial distribution functions,  $G(r)$ , obtained by Fourier transform of the total structure factor  $S(Q)$ , show first neighbors peaks at 2.54, 2.85, 3.36 and 4.20 Å. The peak at 2.54 Å is at the position expected for the nearest neighbor Fe atoms in the dense random packing (DRP) model; the other peaks cannot be correlated to combinations of the radii of Nd (1.82 Å), Al (1.43 Å) or Fe (1.27 Å) atoms as predicted by the DRP model. This disagreement, which is

particular to the case of the present light rare-earth RE–TM alloys, could be ascribed to the development of a new type of disordered structure. Thus, one suggests that the structure consists in a dense random packing of nanometer-sized atomic clusters, the size being dependent on the thickness of the ribbon, i.e. the melt-spinning conditions.

Let's consider atoms like rigid spheres dense randomly packed in a given structure. If we ignore the intensity of the chemical bonding, thus the interatomic distances are equal with the sum of the atomic radii. Considering  $r_{Nd} = 1.82 \text{ \AA}$ ,  $r_{Fe} = 1.27 \text{ \AA}$  and  $r_{Al} = 1.43 \text{ \AA}$ , the theoretical values for Nd–Nd, Nd–Fe, Nd–Al, Fe–Fe, Fe–Al and Al–Al atomic pairs are respectively: 3.64  $\text{\AA}$ , 3.09  $\text{\AA}$ , 3.25  $\text{\AA}$ , 2.54  $\text{\AA}$ , 2.7  $\text{\AA}$  and 2.86  $\text{\AA}$ . Comparing these values with those calculated from experimental data (Table 2) one observes that Fe–Fe values fit very well, whereas the others are larger than experimental ones. This can be explained in the hypothesis of the existence of randomly distributed Fe clusters, while Nd and Al atoms are distributed randomly between these clusters.

Table 2. The interatomic distances (r) and the coordination numbers (N) as a function of x, for  $\text{Nd}_{50}\text{Fe}_{40}\text{Al}_{10}$  melt-spun ribbons, at room temperature.

Thickness, t ( $\mu\text{m}$ )	Fe–Fe		Fe–Nd(Al)		Nd–Nd	
	r ( $\text{\AA}$ )	N	r ( $\text{\AA}$ )	N	r ( $\text{\AA}$ )	N
25	2.54	8.65	2.85	4.85	3.44	5.72
120	2.51	7.69	2.76	7.39	3.38	8.30

Consequently, one expects complex magnetic behavior dependent on thickness and composition. Values of the magnetization measured in a field of 800 kA/m and coercive field obtained at room temperature for  $\text{Nd}_{50}\text{Fe}_{40}\text{Al}_{10}$  amorphous samples are given in Table 3. The large values of the coercive field can be explained by assuming the existence of a microstructure consisting of very small magnetic clusters, whose size approaches a single magnetic domain, dispersed in the amorphous matrix, in agreement with the neutron diffraction results as well as with the previous results obtained for melt spun Nd–Fe amorphous alloys [11]. The size and the composition of these magnetic clusters are strongly dependent on the cooling rate. The sizes of these magnetic clusters are small enough and cannot be evidenced by XRD measurements.

Table 3. Magnetic characteristics of  $\text{Nd}_{50}\text{Fe}_{40}\text{Al}_{10}$  amorphous ribbons and rods, at room temperature.

Sample	Thickness (mm)	$\mu_0 M_{\{10 \text{ kOe}\}}$ (T)	$iH_c$ (kA/m)
Amorphous ribbon	0.030	0.33	64
Amorphous ribbon	0.055	0.24	123
Amorphous ribbon	0.085	0.25	226
Amorphous ribbon	0.105	0.32	274
Amorphous ribbon	0.142	0.23	286
Amorphous rod	0.6	0.25	244
Amorphous rod	1.8	0.24	246

The higher values obtained for the coercive field of the thick amorphous ribbons comparatively with thin ones are related to the more relaxed microstructure developed in the first ones. It is worthwhile to note that the magnetization for the ribbon of 105  $\mu\text{m}$  is almost the same like for the ribbon 30  $\mu\text{m}$ , whereas the coercive field is 4 times larger. This behavior can be explained by the largest degree of structural disorder existent in the ribbon of 105  $\mu\text{m}$ , in agreement with the largest crystallization energy obtained from DSC curves. In these conditions, an external applied field causes the alignment of more magnetic domains relative to its direction. The microstructure is more homogenous in amorphous rods due to their dimensions and lower cooling rates and consequently the values obtained for coercive field are smaller than for the thick ribbons.

$\text{Nd}_{90-x}\text{Fe}_x\text{Al}_{10}$  ( $x = 35 - 50$ ) amorphous alloys exhibit large coercive fields at room temperature, even for low applied fields, regardless of their thickness and preparation techniques. The magnetization increases about 2 times by increasing the Fe content from 35 to 50 at. %, regardless of the amorphous samples shape, the same behavior being observed for high fields up to 9 T. The coercive field presents a strong dependence on the composition. The on-set of crystallization in the  $\text{Nd}_{40}\text{Fe}_{50}\text{Al}_{10}$  thick ribbon results in the decrease of the magnetization, while the coercive field has almost the same value as that obtained for fully amorphous thick ribbons with a less content of Fe because of the existence of the amorphous residual phase. Thus, the large coercive fields of Nd-Fe-based ternary bulk amorphous alloys are related to the existence of the amorphous phase, its disappearance leading to the drastically decrease of the coercive field and moreover, to the disappearance of the ferromagnetic properties, as we will see in the following. The decrease of the Fe content results in the decrease of the coercive field of about 2 times for thin amorphous ribbons and in its increase of about 2 times for amorphous cast rods. For thick amorphous ribbons the coercive field is almost the same, regardless of the Fe content. For higher external fields (larger than 3 T) the coercive field doesn't change significantly with the Fe content for each different type of ribbon or for cast rods. The difference in the absolute value of the coercive field as a function of the amorphous samples' thickness results from the volume rate between Fe-based magnetic clusters and the homogenous Nd-rich matrix through the cooling rate.

Thus,  $\text{Nd}_{90-x}\text{Fe}_x\text{Al}_{10-y}\text{Si}_y$  bulk amorphous alloys are structurally "glassy" but magnetically "granular". The granular magnetic structure consists in Fe-based nanosized clusters dispersed in amorphous Nd-rich matrix. Due to their very small dimensions they cannot be evidenced by X-ray diffraction measurements, but their presence is proved by the specific magnetic behavior of these bulk amorphous alloys, especially by the high coercive fields in the as-quenched state and the dependence on the cooling rate. The composition and size of the magnetic clusters as well as the composition of the matrix in which the clusters are embedded are very sensitive to the preparation conditions, mainly the cooling rate and the thermal history of the molten alloy. Fe-based magnetic clusters are coupled between them through the amorphous matrix and the exchange coupling is strongly influenced by the magnitude of the  $\text{Nd}^{3+}$  single ion local anisotropy. Whereas at low temperatures the anisotropy plays the predominant role in the macroscopic magnetic response of the system, the increase of the temperature diminishes its effect and the main role is attributed to the ferromagnetic exchange energy. At low temperature, the local anisotropies of the  $\text{Nd}^{3+}$  ions are very strong and oriented randomly, thus they can "freeze" randomly the magnetic moments of Fe and Nd. The anisotropy axis corresponding to the Fe-Nd pairs are oriented randomly, and a small external field is not enough to align them. The AC-susceptibility measurements as well as the variation of the coercive field on temperature in the range 4 – 300 K [12] indicate magnetic transitions that suggest different local arrangements of the Nd atoms, similar to dhcp (double hexagonal compact) and fcc crystalline phases. The first transition appears around 10 K and seems to be related to the Néel transition temperature of the Nd antiferromagnetic. Another magnetic transition is observed around 70 K and is due to the transition from a completely disordered magnetic phase to a sperrimagnetic non-collinear one.

Different magnetic structures can be obtained depending on temperature and the predominant coupling between Fe and Nd atoms. This is probably the explanation for the lack of the hysteresis loop at temperatures between 10 and 100 K and low external fields ( $< 1$  T) [12]. In this range of temperatures Nd-rich matrix and Fe-based magnetic clusters are completely uncoupled, but the exchange coupling within the clusters still exist. If from any reason, the coupling between clusters is not possible, the macroscopic response of the system is weakly ferromagnetic. The maximum of the coercive field is attained at that temperature at which the anisotropy energy and the exchange energy have similar values, i.e. the magnetic clusters have the size of the single magnetic domain [13]. Taking in consideration the critical size for the Fe single domain of about 1000 Å and the strength of the local anisotropy of the  $\text{Nd}^{3+}$  ions results that the Fe magnetic moment is not aligned on a direction but forming a cone with an angle of about  $30^\circ$  [14]. Thus, the magnetic structures are non collinear and the critical size of the single magnetic domain is smaller than 100 nm.

In Nd-Fe-based thin amorphous ribbons, due to their reduced dimensions, high cooling rate (which does not allow the structural relaxation) and thermal effects, the system tends to a superparamagnetic regime at room temperature, and consequently the coercive field is not very large.

It is known that in materials containing single magnetic domains the magnetization is due mainly by the magnetic moments rotations. If the value of the applied field is not large enough, the measured hysteresis loops are minor loops, and the measured magnetization is far from its saturation. This effect is more pronounced in materials in which the magnetic anisotropies play an important role in magnetization processes. Nd-Fe-based bulk amorphous materials with strong local random magnetic anisotropy of the  $\text{Nd}^{3+}$  ions, which becomes stronger by decreasing the temperature, belong to this class of materials.

A proof of the role of the magnitude of the applied field on the magnetic response of the system is shown in Fig. 4 for  $\text{Nd}_{50}\text{Fe}_{40}\text{Al}_{10}$  amorphous ribbons 25 and 120  $\mu\text{m}$  in thickness.

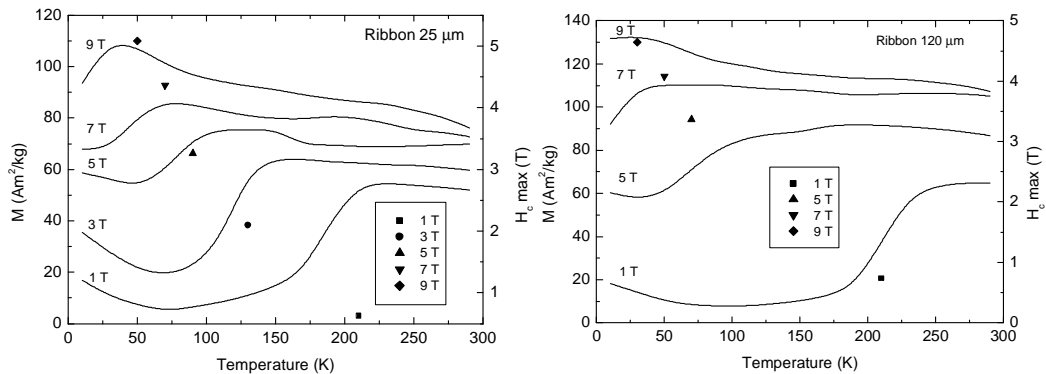


Fig. 4. The magnetization and the maximum of the coercive field versus temperature and applied field for  $\text{Nd}_{50}\text{Fe}_{40}\text{Al}_{10}$  amorphous melt-spun ribbons (the coercive field is represented by symbols).

As larger the applied field as smaller the temperature at which the coercive field attains its maximum. One observes also that the magnetization exhibits different behavior for applied fields no large enough to align the magnetic moments parallel to its direction, i.e. to be large enough to overload the anisotropy energy given by the  $\text{Nd}^{3+}$  ions anisotropy.

Thermomagnetic measurements (after cooling without field or after cooling in an external field) at temperatures above 300 K indicate the co-existence of two types of magnetic order: spin-glass-like or cluster-glass-like short-range order within the clusters and long-range order ferromagnetic order like a response of the exchange coupling between clusters [15]. Consequently, the magnetic structure consists in randomly distributed non-collinear short-range magnetic ordered regions.

#### 4. Perspectives

Despite the considerable progress achieved in recent years concerning the knowledge of the atomic structure of amorphous alloys and concerning the understanding of their basic magnetic properties, several unsolved problems were encountered in the field of bulk magnetic amorphous alloys. There are still many questions related to the microstructure of these materials and its interplay with magnetic properties, especially for Nd-Fe-based high coercivity bulk amorphous alloys. The magnetic ground states of Nd-Fe-based cluster amorphous alloys and non-collinear structures existent in these materials are far from being fully characterized. These problems and others make the study of the magnetic properties of bulk amorphous alloys a fascinating field of research. Bulk magnetic amorphous alloys are interesting also for the field of engineering applications.

#### References

- [1] H. S. Chen, *Acta Metall.*, **22**, 1505 (1974).
- [2] A. Inoue, J. S. Gook, *Mater. Trans., JIM*, **36**, 1180, 1282 (1995).
- [3] A. Inoue, Y. Shinohara, J. S. Gook, *Mater. Trans., JIM*, **36**, 1427 (1995).

- [4] A. Inoue, T. Zhang, W. Zhang, A. Takeuchi, Mater. Trans., JIM, **37**, 99 (1996).
- [5] A. Inoue, T. Zhang, A. Takeuchi, W. Zhang, Mater. Trans., JIM, **37**, 627 (1996).
- [6] D. A. Keen, R. L. McGreevy, R. I. Bewley, R. Cywinski, Nucl. Instrum. Meth. Phys. Res., **A354**, 48 (1995).
- [7] H. Chiriac, N. Lupu, J. Non-Cryst. Solids, **250-2**, 751 (1999).
- [8] H. Chiriac, N. Lupu, J. Magn. Magn. Mater., **215-216**, 394 (2000).
- [9] H. Chiriac, N. Lupu, Physica B: Condens. Matter, **299**, 293 (2001).
- [10] H. A. Alperin, W. R. Gillmor, S. J. Pickart, J. J. Rhyne, J. Appl. Phys., **50**, 1958 (1979).
- [11] J. J. Croat, IEEE Trans. Magn., **MAG-18**, 1442 (1982).
- [12] H. Chiriac, N. Lupu, K. V. Rao, R. E. Vandenberghe, IEEE Trans. Magn., **37** (2001) 2509.
- [13] B. D. Cullity, Introduction to Magnetic Materials, Addison\_Wesley Publishing Company (1972) p. 385.
- [14] K. Moorjani, J. M. D. Coey, Magnetic Glasses, Elsevier, Amsterdam (1984).
- [15] H. Chiriac, N. Lupu, K. V. Rao, Scripta Mater., **44**, 1379 (2001).